

Towards Long-Range 3D Object Detection for Autonomous Vehicles

Ajinkya Khoche^{1,2}, Laura Pereira Sánchez³, Nazre Batool², Sina Sharif Mansouri² and Patric Jensfelt¹

Abstract—3D object detection at long-range is crucial for ensuring the safety and efficiency of self-driving vehicles, allowing them to accurately perceive and react to objects, obstacles, and potential hazards from a distance. But most current state-of-the-art LiDAR based methods are range limited due to sparsity at long-range, which generates a form of domain gap between points closer to and farther away from the ego vehicle. Another related problem is the label imbalance for faraway objects, which inhibits the performance of Deep Neural Networks at long-range. To address the above limitations, we investigate two ways to improve long-range performance of current LiDAR-based 3D detectors. First, we combine two 3D detection networks, referred to as range experts, one specializing at near to mid-range objects, and one at long-range 3D detection. To train a detector at long-range under a scarce label regime, we further weigh the loss according to the labelled point’s distance from ego vehicle. Second, we augment LiDAR scans with virtual points generated using Multimodal Virtual Points (MVP), a readily available image-based depth completion algorithm. Our experiments on the long-range Argoverse2 (AV2) dataset indicate that MVP is more effective in improving long range performance, while maintaining a straightforward implementation. On the other hand, the range experts offer a computationally efficient and simpler alternative, avoiding dependency on image-based segmentation networks and perfect camera-LiDAR calibration.

I. INTRODUCTION

As autonomous vehicles continue to make significant strides toward widespread adoption, ensuring their safety and reliability remains a paramount concern. One crucial aspect is the range of perception, a vital capability that enables self-driving cars to perceive and understand their surroundings accurately. While the need for long-range perception is apparent in various driving scenarios, it becomes especially critical for heavy-duty trucks on highways, where vehicles encounter potential hazards at high speeds requiring fast reaction time.

A standardized safety assurance framework has been provided by authors in [1] for determining a safe longitudinal distance, considering factors such as comfortable deceleration, vehicle speed, and reaction time. Based on their findings, an object detection range exceeding 300 meters is needed to ensure a safe braking distance for autonomous trucks in highway scenarios. Yet, the problem of 3D object detection at such ranges remains largely unexplored. At present, no publicly available datasets cover such a large

range or provide data recorded on trucks. In our study, we use the Argoverse2 (AV2) dataset [2], which provides annotations up to 225 m. We define objects lying beyond 100 m to be *long-range*, and those within 100 m to be *mid-range*.

At present, the realm of 3D object detection is largely led by methods relying on Light Detection and Ranging (LiDAR) technology, as it excels in delivering precise point-based estimations of the environment. While state-of-the-art methods have showcased notable results in the context of mid-range detection, they often do not discuss findings for long-range detection or, when presented, exhibit poor performance in such scenarios [3], [4], [5]. We identify two primary issues that are currently constraining existing methods. The first issue is that the LiDAR point cloud gets increasingly sparse with distance, as shown in Figure 2a. This causes a form of domain gap, which has been studied in the context of sim2real or sensor-to-sensor mapping applications [6], but not with regards to long range detection. Studies have suggested relying on camera-based methods for object detection beyond a specific range [5]. Alternatively, utilization of a dedicated network designed for processing long-range point data has been proposed [4]. Another consequence of LiDAR sparsity is that a LiDAR based detector lacks the necessary information to make precise predictions.

The second issue is related to the uneven distribution of

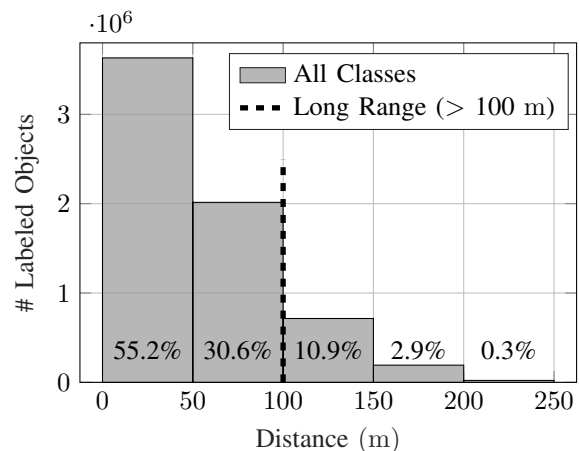


Fig. 1: Number of labeled objects for all categories as a function of range for the training set of the AV2 dataset. The first two bins, which we refer to as mid-range, contain 85.8% of the events in the data set. The 100-150 m range contains most of the long range objects, 10.9%, leaving only 3.2% objects over 150 m.

*This work was supported by the research grant PROSENSE (2020-02963) funded by VINNOVA.

¹KTH Royal Institute of Technology, Stockholm 10044, Sweden. Corresponding author’s e-mail: khoche@kth.se

²Autonomous Transport Solutions Lab, Scania Group, Södertälje, SE-15139, Sweden

³Stockholm University, Fysikum, Stockholm 114 21, Sweden.

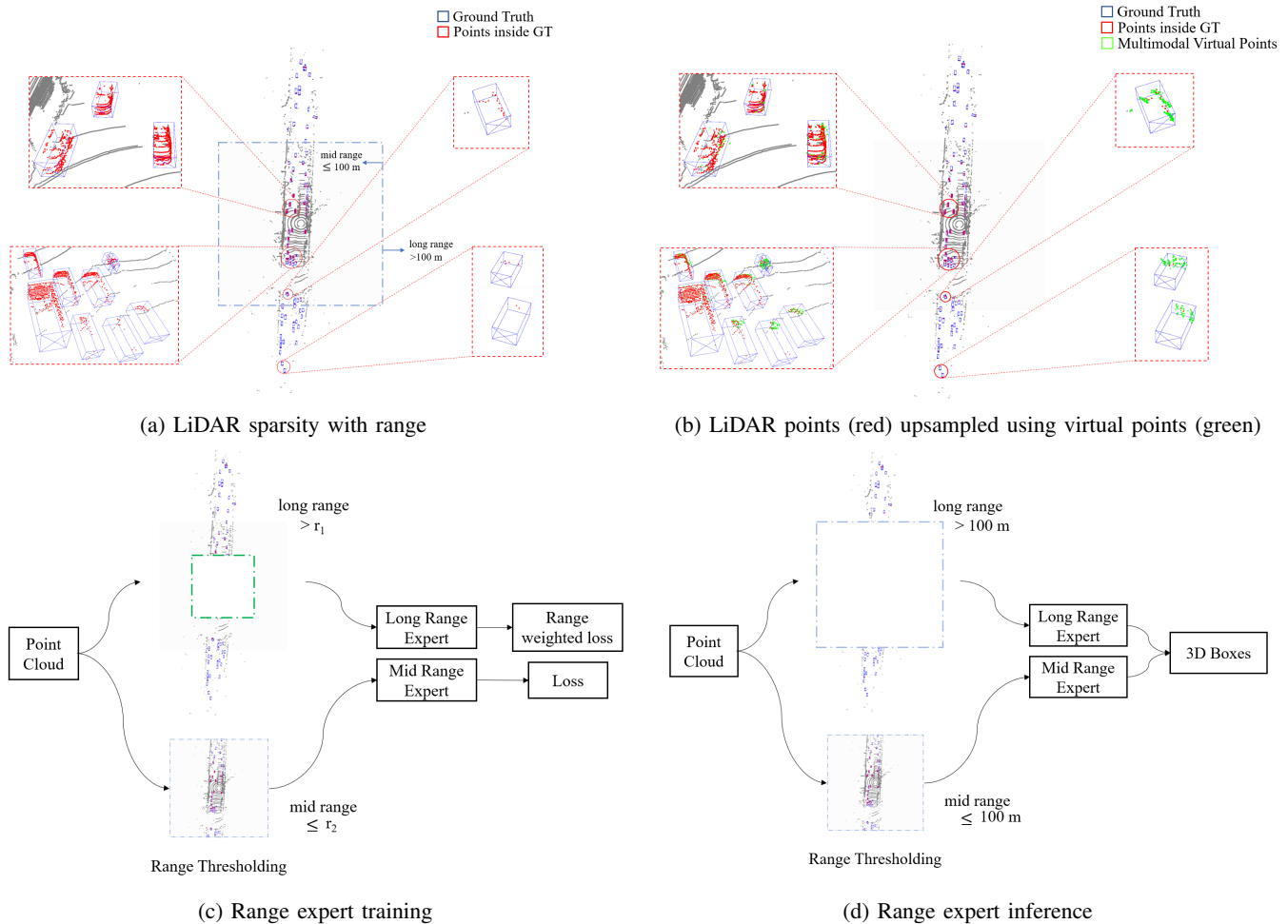


Fig. 2: Increased LiDAR sparsity with distance from ego vehicle is one of the major challenges facing long range (>100 m) 3D object detection. (a) shows that the two vehicles parked far away from the ego vehicle have fewer LiDAR points, as well as appear different compared to those parked nearby. To address this problem, we analyze two approaches: (b) adding virtual points during training, and (c) training two neural networks, one specializing in mid-range object detection, and one for detecting long-range objects. The parameters $r_1, r_2 \in [0, 250]$, represented by the green and blue box respectively, delimit a subset of points used for training the long and mid-ranged experts respectively. Mid-range expert uses points within a distance r_2 of the ego vehicle, while points outside the distance r_1 are used to train the long-range expert. (d) During inference, we combine outputs from the two networks, such that the long-range detector contributes detections beyond blue box (>100 m), and the mid-range detector contributes detections within blue box.

labeled objects across different ranges for training. Partially as a result of increasing LiDAR sparsity with distance, there are fewer annotations at long-range, as shown in Figure 1. Although many new datasets have been released covering long-range annotations partially, they do not specifically focus on improving label imbalance for long-range annotations [7], [8], [9], [10].

In this work, we present the first comprehensive evaluation of 3D object detectors for distances beyond 100 meters, addressing a critical gap in the literature. Our novel contributions include:

- The integration of recent advancements in image-based depth completion to enhance long-range 3D object detection. We generate virtual points for objects identified by an image-based segmentation network, as illustrated

in Fig. 2b. The increased density of points significantly improves the detection performance at both mid and long ranges.

- The development and training of two specialized networks designed as range experts: one focused on mid-range and the other on long-range detections. During inference, we merge their outputs, ensuring each network operates within its optimal detection range. This approach is detailed in our proposed detection pipeline (refer to Figs. 2c and 2d).
- A strategy to address label imbalance by weighting labels based on their distance from the ego vehicle. During training, higher weightage is assigned to the loss component of a faraway labeled object compared to the one nearer to the ego vehicle. This weighing is inversely

proportional to the number of annotations in a particular range bin.

- Moreover, we conducted a comparative analysis of our range expert networks against a detector trained with virtual points using the long-range AV2 dataset. We also compare our best performing network to other state-of-the-art methods, observing significant improvements.

The rest of this article is structured as follows. Section II describes the related work in the field of 3D Object Detection, with a focus on long range detection. Section III describes range experts and outlines their training scheme for long range detection. Section IV presents the experimental results and discusses their implications, while limitations, concluding remarks and future work are discussed in Section V and Section VI.

II. RELATED WORK

This section presents the state-of-the-art in long-range 3D object detection and image based depth completion, as well as briefly describes the methods in fully sparse detection, most related to our work.

A. Long Range 3D Object Detection

Point based or grid based methods utilizing sparse convolutions [11], [12] present interesting opportunities for long range 3D detection. VoxelNext [13] adds downsampling layers to existing 3D sparse convolution blocks to enlarge the receptive field, followed by pruning voxels with low feature magnitude, striking a balance between performance and computation. IA-SSD [14] first estimates per-point semantics and a centroid aware feature indicating closeness to a box center, and uses it to sample top k points. While both methods demonstrate generally good performance, the feature pruning might remove information for long range objects.

Recently, there has been growing interest in multi-modal fusion based methods for long range detection. In Far3Det [5], the authors report that fusion based methods outperform LiDAR only methods, given that the inaccuracies in camera based depth estimation are taken into account during evaluation. They propose range adaptive NMS thresholds and a straight-forward late fusion scheme, where camera-based detections are preferred beyond certain range. However, at present many camera based methods for 3D detection rely on converting image features into bird’s eye view (BEV) representations, which poses significant computational challenges for long range [15]. Zhang et. al. [4] classify and cluster the points inside frustum obtained from image based segmentation networks, and design a novel FFNet to regress the 3D bounding box. Fully Sparse Fusion (FSF) [3] similarly uses image to cluster LiDAR points. They further utilize the Fully Sparse Detector (FSD) [16] network to filter noisy points at mask boundaries. The image segmented cluster is fused with LiDAR segmented clusters for feature extraction and box prediction. To the best of our understanding, none of the methods listed above discuss or

present results specifically at long range, i.e. above 100 m distance.

B. Fully Sparse Detectors

FSD [16] is among the first computationally efficient point based methods. It overcomes the drawbacks of neighborhood querying and multiple cluster assignments faced by previous methods, by first pre-segmenting and voting on the point cloud using a SparseUNet [12]. Clustering [17] on these voted centers assigns a unique grouping to every point, avoiding ambiguity. This is followed by designing a novel Sparse Instance Recognition (SIR) module to extract cluster features and predict boxes.

To account for noise in clustering, FSDv2 [18] instead voxelizes the voted centers to form *virtual voxels* to capture the ambiguity/noise in clustering. Thereafter multi-scale features from a sparseUNet decoder are fused with those from virtual voxels and real voxels (obtained from the foreground segmented points). We use FSD and FSDv2 as backbones for mid range and long range experts, due to their state-of-the-art results on long range 3D object detection, as well as their computational efficiency.

C. Image Based Depth Completion

Rich semantic information from image based 2D detectors can provide valuable cues for long range objects, such as rough estimation of object center [4], [19], enhanced feature representations [20], [21]. An intriguing research direction, which directly targets the LiDAR sparsity problem is image-based depth completion. Prior research has explored this approach to a lesser extent in the context of long-range 3D detection. In the work by Zhang et al. [22], a Deep Neural Network (DNN) is used to estimate surface normals and occlusion boundaries, and combine them with raw depth measurements for depth completion. The work presented in [23] uses classical image processing operations like dilation with custom designed kernel, hole filling, and median filtering to fill the depth map.

The method Multimodal Virtual Points (MVP) [24] first uses an image based instance segmentation network to generate instance masks where s pixels are randomly sampled without repetition for each mask. Next, for each pixel, the nearest LiDAR point, obtained by projecting the point cloud onto mask using intrinsic and extrinsic parameters, is located. The nearest LiDAR points are then used to assign depth to these s pixels, which are lastly unprojected back to 3D to obtain the virtual points. Among existing approaches, the MVP stands out as one of the top-performing methods, notable for its efficacy and simplicity.

III. METHODOLOGY

Due to the increase in sparsity of the LiDAR point cloud as a function of the distance, objects at different distances appear to be radically different. To tackle this issue, we investigate two approaches: Firstly, we use MVP, as described in previous section, to generate virtual points. These virtual points are then fused with the LiDAR data before training

FSD and FSDv2. Second, we train two specialized versions of the detector, each optimized for a specific distance domain: one for mid-range and another for long-range points. This specialization is achieved through range thresholding, which allows each detector to focus on learning features relevant to its designated range domain. The long-range detector, in particular, employs a weighted loss function that accounts for the object’s distance. During inference, we employ a late fusion strategy to integrate the outputs from both range experts. The following sections delve into the detailed implementation of our range experts, their training process, and the fusion mechanism

A. Notation

The set $\mathcal{P} = \{(x_i, y_i, z_i, f_i), i \in \mathbb{N}\}$ represents a point cloud in \mathbb{R}^4 . Range experts are denoted by $F_{r_1-r_2}$ where F is the DNN used for training, and $r_1, r_2 \in \mathcal{R} = \{0, 50, 100, 150, 200, 250\}$ are the range thresholds (in meters) within which it is trained. For a range threshold r , we consider a square axis aligned region where r denotes the distance from the origin to the border along the x or y axis. The set \mathcal{R} further defines a set of bins \mathcal{B} separated by fixed length interval of 50 m. The maximum range is set to 250 m for the AV2 dataset. Specifically, $F_{r_1-r_2}$ is trained to perform inference for points $p \in \mathcal{P}$ such that $r_1 \leq r \leq r_2$. In this paper, we consider F_{0-250} as the baseline model upon which we build our contributions. Furthermore, we denote $F_{r_1-r_2}^w$ as an expert trained using range weighing.

B. Range Thresholding

Range thresholding consists of training the network using only a subset of points within a specific range interval $r_1 - r_2$. The resulting networks are referred to as range experts. Given the large difference in the number of labeled objects as a function of their distance, which was illustrated in Fig. 1, a mid-range expert is not crucial since the baseline, F_{0-250} , already performs fairly well as a mid-range detector, however, specialised long-range experts are clearly required. We evaluate the performance of the long-range experts as a function of the range thresholding values. Similarly to [25], which tests range thresholds on BEV methods, we observe that as we increase the lower bound for range thresholding, the network performs poorer compared to baseline at long range. This is because, as seen in Fig. 1, we end up discarding larger and larger proportion of labels while training, and the network does not have enough data to learn from. This problem inspired us to also implement the range weighing.

C. Range Weighing

Range weighing is aimed at compensating for the imbalance of labeled objects at large distances, which was illustrated in Fig. 1. This is achieved by increasing the impact of objects that are further away on the loss function. In order to strike a balance between range thresholding and retaining sufficient labels for training, we propose range adaptive weighing. The loss corresponding to a predicted

cluster/virtual voxel is weighed according to its range. In general, the label weight w_b for the range bin b is given by:

$$w_b = \frac{N}{n_b \times B} \quad (1)$$

where N is the total number of labels for all classes in the dataset, n_b is the number of objects in range bin b and B is the number of bins covered by the range expert. The weight w_b is applied to the Focal Loss [26] and L_1 Loss [27], which are used as classification and regression losses for the prediction head for bounding boxes. The other loss terms remain unchanged (refer to [16], [18] for more details). The range weights for both mid and long range experts for different values of range thresholding r_1 and r_2 are denoted in Table I.

TABLE I: Range weights for different values of range thresholds. r_1 and r_2 are lower and upper limits for thresholding.

r_1	r_2	0-50	50-100	100-150	150-200	200-250
0	250	0.360	0.661	1.852	6.486	52.332
50	250	0	0.367	1.030	3.607	29.103
100	250	0	0	0.440	1.542	12.440

D. Late Fusion

We studied various combinations of range thresholding and range weighing using FSD [16], and chose F_{0-100} and F_{50-250}^w as the mid and long-range experts. During inference, the detections from the mid and long-range experts are combined such that the mid-range expert contributes detections with centers from 0-100 meters, whereas the long-range expert contributes detections from 100-250 meters.

IV. EXPERIMENTS

A variety of experiments and ablation studies are documented in this section. We assess the impact of our individual contributions and compare the best performing model to other state-of-the-art methods from the literature.

A. Experimental Setup

Dataset: We conduct experiments on the AV2 perception dataset, which contains 1000 scenes divided into 700 for training and 150 each for validation and testing. Each scene captures roughly 15 s of data on two 32-beam LiDARs at 10 Hz but with a 180° difference in spinning angle, seven color cameras and two forward-facing stereo cameras at 20 Hz, providing a surround view of the vehicle. Objects of interest are annotated at 10 Hz among 30 categories, up to 225 m away from the ego vehicle.

Implementation Details: We base our implementation on FSD [16], which is in turn developed using mmdetection3d library [28]. We start with a pre-trained FSD and train for six epochs using Class-balanced grouping and sampling (CBGS) [29]. Thereafter we train the mid and long-range experts for further 3 epochs and combine them, as explained in Section III. The combined network is referred to as range expert (or RE for brevity). For MVP, We use Hybrid Task Cascade (HTC) [30] pretrained on NuImages dataset as

the default 2D image segmentor for generating the virtual points. Thereafter, we further train an FSD using these virtual points for 3 epochs with CBGS. We use the same data augmentations and learning parameters as [16] and train on eight Nvidia A-100 GPUs.

Metrics: AV2 uses mean Average Precision (mAP) and Composite Detection Score (CDS) scores for evaluating 3D detection. In this work, we report the mAP, which is defined as the mean of Average Precision (AP) across C classes, where AP_j for class j is the discrete integral of precision $p_d(a)$ interpolated at 100 discrete recall values $a \in [0, 1]$, averaged across four chosen distance thresholds d (in meters).

$$mAP = \frac{1}{C} \sum_{j=1}^C AP_j \quad (2)$$

$$AP_j = \frac{1}{4} \sum_{d=\{0.5,1,2,4\}} \frac{1}{100} \sum_{a=\{0,0.05,\dots,1\}} p_d(a) \quad (3)$$

Unless otherwise specified, we use an evaluation range of 0-250 m in our experiments.

B. Performance Breakdown

In order to assess the impact of range experts and MVP towards enhancing 3D object detection, a detailed performance breakdown, shown in Table II, is performed.

TABLE II: mAP comparison (all classes). †: provided by authors [16]. *: re-trained by us. RE: Range Experts. MVP: Multimodal Virtual Points.

Method	0-250	0-50	50-100	100-150	150-200	200-250
FSD†	28.5	43.7	12.6	3.3	1.0	0.3
FSD*	29.8	44.9	14.3	4.1	1.0	0.3
FSD*+RE	30.2	45.5	14.8	4.3	1.2	0.3
FSD*+MVP	31.5	46.4	16.6	5.4	1.8	0.5
FSD*+RE+MVP	31.9	46.9	16.9	5.8	2.0	0.5

To guarantee a fair comparison, we re-train the baseline networks for six epochs using CBGS, which we denote by *. We also provide the performance reported by the authors of the baseline for completeness, denoted by †. For FSD, we reduce the minimum points for clustering from two to one, to enable clustering at long range. It’s observed that using CBGS seems to slightly benefit long range performance. Compared to FSD*, RE and MVP contribute to 0.4% and 1.7% improvement overall. But it becomes difficult to access the performance beyond 100 m range. Upon analysing the class distribution across different range bins, we found that roughly 50-70% objects belong to a single class category: vehicle. Especially beyond 100 m, other categories have very few annotations. Due to this their class-wise AP falls close to zero, making the mAP very low. In order to remedy this, we present the performance breakdown with only the AP for vehicle class in table Table III.

For distances exceeding 100 meters, range experts contribute to an increase of up to 1.7% in vehicle AP, whereas MVP yields a significantly greater enhancement, achieving an increase of up to 9.3%. This marked improvement

TABLE III: AP comparison (Vehicle class only). †: provided by authors [16]. *: re-trained by us. RE: Range Experts. MVP: Multimodal Virtual Points.

Method	0-250	0-50	50-100	100-150	150-200	200-250
FSD†	70.5	88.9	59.7	26.8	12.1	2.6
FSD*	71.5	89.0	61.7	29.2	13.9	3.6
FSD*+RE	71.9	89.0	62.5	30.0	15.6	3.4
FSD*+MVP	74.5	89.0	66.0	39.2	23.2	6.0
FSD*+RE+MVP	74.5	89.2	66.0	39.3	23.2	6.0

is primarily due to MVP’s application of virtual points upsampling during the evaluation phase, a technique not employed by other approaches. Furthermore, MVP relies on precise camera-LiDAR calibration. Any misalignments in the extrinsic calibration process can result in inaccuracies in depth completion and the potential exclusion of objects when nearby LiDAR points are absent. This limitation is particularly notable for distant objects and can significantly impact the overall performance of the network.

The integration of MVP with range experts yields a modest improvement in overall mAP, however, it appears to have a limited effect on enhancing vehicle AP. This outcome may stem from MVP’s capability to bridge the domain gap between mid-range and long-range points, reducing the contributions of range experts. Our results underscore the substantial room for improvement within the current state-of-the-art for long-range 3D detection.

C. State-of-the-art Comparison

We compare our best performing model (Baseline*+RE+MVP) to various state-of-the-art algorithms from the literature, as shown in Table IV. We use FSD and FSDv2 as our baselines. The evaluation range is set to 0-200 m to enable a fair comparison to other methods. Notably, our models outperform their respective baselines and surpass all previously proposed state-of-the-art methods. Although improvements span across many classes, they are especially notable for vulnerable road users (2-3% for pedestrians, motorcyclist, bicyclist) and small objects (3-10% for motorcycle, bicycle and construction cones). Equally interesting is the drop in performance for some classes, as compared to FSDv2 baseline. This drop could be caused by the noise in the virtual point generation process, which in turn is caused by noisy masks generated by the 2D segmentor, for classes it is not trained on. As mentioned earlier, we use an off-the-shelf 2D segmentor (HTC [30]) trained on the NuImages dataset. We perform a one-to-one mapping between NuImage classes and their best match among the 26 classes in the AV2 dataset. Inevitably, some classes not covered by this scheme don’t improve (like box truck), or even get worse if mislabeled (eg. wheelchair, sign, stop sign etc.).

D. Ablation Studies

Runtime Comparison:

The runtime is evaluated on a single A-100 GPU. Following [18], we set the batch size to 1 and evaluate the

TABLE IV: Comparison to state-of-the-art on AV2 validation split. The evaluation range is 0-200 m. †: provided by authors of AV2 [2]. ‡: reimplemented by FSD [16]. *: re-trained by us. RE: Range Experts. MVP: Multimodal Virtual Points [24]. C-Barrel: construction barrel, MPC-Sign: mobile pedestrian crossing sign, A-Bus: articulated bus, C-Cone: construction cone, V-Trailer: vehicular Trailer, W-Device: wheeled device, W-Rider: wheeled rider.

Method	mAP	Vehicle	Bus	Pedestrian	Stop Sign	Box Truck	Bollard	C-Barrel	Motorcyclist	MPC-Sign	Motorcycle	Bicycle	A-Bus	School Bus	Truck Cab	C-Cone	V-Trailer	Sign	Large Vehicle	Stroller	Bicyclist	Truck	MBT	Dog	Wheelchair	W-Device	W-Rider
CenterPoint† [31]	13.5	61.0	36.0	33.0	28.0	26.0	25.0	22.5	16.0	16.0	12.5	9.5	8.5	7.5	8.0	8.0	7.0	6.5	3.0	2.0	14.0	14.0	1.0	0.5	0	3.0	0
CenterPoint‡	22.0	67.6	38.9	46.5	16.9	37.4	40.1	32.2	28.6	27.4	33.4	24.5	8.7	25.8	22.6	29.5	22.4	6.3	3.9	0.5	20.1	22.1	0	3.9	0.5	10.9	4.2
VoxelNet [13]	30.7	72.7	38.8	63.2	40.2	40.1	53.9	64.9	44.7	39.4	42.4	40.6	20.1	25.2	19.9	44.9	20.9	14.9	6.8	15.7	32.4	16.9	0	14.4	0.1	17.4	6.6
FSF [3]	33.2	70.8	44.1	60.8	27.7	40.2	41.1	50.9	48.9	28.3	60.9	47.6	22.7	36.1	26.7	51.7	28.1	12.2	6.8	25.0	41.6	-	-	-	-	-	-
FSD [16]	28.2	68.1	40.9	59.0	29.0	38.5	41.8	42.6	39.7	26.2	49.0	38.6	20.4	30.5	14.8	41.2	26.9	11.9	5.9	13.8	33.4	21.1	0	9.5	7.1	14.0	9.2
FSD*+RE+MVP	31.9	74.5	42.1	69.2	32.0	39.1	53.3	58.7	50.1	27.4	55.9	46.1	21.2	30.5	20.2	54.8	26.4	12.0	6.2	15.9	42.6	21.4	0	1.9	2.3	17.2	9.5
FSDv2 [18]	37.6	77.0	47.6	70.5	43.6	41.5	53.9	58.5	56.8	39.0	60.7	49.4	28.4	41.9	30.2	44.9	33.4	16.6	7.3	32.5	45.9	24.0	1.0	12.6	17.1	26.3	17.2
FSDv2*+RE+MVP	38.5	78.5	48.4	72.8	43.0	41.5	56.1	65.1	60.2	48.8	63.8	53.2	29.6	40.6	30.3	55.9	31.3	16.2	7.3	30.3	48.9	23.8	0	14.6	1.4	25.0	14.7

TABLE V: Runtime (msec) and memory (GB) comparison. *: re-trained by us.

Method	Runtime (msec)	Memory (GB)
FSD*	72	2.9
FSD* + RE	164	3.5
Mask RCNN + FSD* + MVP	505	14.5
HTC + FSD* + MVP	1800	27.9

average runtime for 1000 samples on the AV2 validation set, without runtime optimizations. The range experts incur more than twice the runtime cost, and comparable memory consumption compared to FSD. This considers a naive implementation where the mid-range and long-range experts are run sequentially. On the other hand, one could run the mid-range and long-range experts in parallel, in which case their runtime will be comparable to FSD and the memory consumption will double.

MVP relies on masks generated by an image segmentation network for virtual point generation. On the AV2 dataset with 7 cameras, this process takes approximately 425 msec for Mask RCNN and 1720 msec for HTC networks, respectively. While it is important to note that this analysis may depend on specific hardware and implementation factors, the key insight remains clear: when hardware availability is not a constraint, MVP emerges as an attractive choice for improving long-range 3D detection performance. However, in cases where hardware resources are limited, range experts offer a cost-effective alternative to achieve comparable improvements.

Effect of image segmentation: To analyze the impact of the image segmentation backbone on the performance of virtual point generation for MVP, we replace HTC [30], the default 2D segmentor, with Mask RCNN [32], another widely recognized image segmentation model. The results, as displayed in Table VI, reveal a slight improvement in 3D mAP when using Mask RCNN compared to HTC, despite the latter achieving higher 2D mask and bounding box mAP scores. This observation suggests that while both segmentors exhibit robust performance in detecting mid-range objects, HTC excels in identifying smaller objects. Some of these small objects may exist at considerable distances, beyond the

reach of LiDAR points, making it impossible for a LiDAR-only detector to detect them.

TABLE VI: Effect of 2D backbone on mAP performance for FSD*+MVP.

Method	2D mAP		3D mAP
	Mask	Box	
HTC [30]	46.4	57.3	31.5
Mask RCNN [32]	38.4	47.8	31.8

V. LIMITATIONS

Firstly, the effects of fusing data from active LiDAR sensors with passive camera sensors, most of which employ rolling shutters, need to be further investigated. This limitation is especially pertinent when dealing with highly dynamic objects, as they can appear differently in each sensor’s data, leading to further mismatch during depth completion. Also, we did not investigate scenarios where large objects, like trucks with trailers, span our range boundaries. In such cases, short-range and long-range networks may yield separate bounding boxes for the same object, necessitating fusion.

VI. CONCLUSIONS AND FUTURE WORK

In this work, we identify two key problems that 3D Object Detectors face at long range: LiDAR sparsity, causing a form of domain gap, and label imbalance between mid and long range objects. To address these problems, we analyze two solutions: a combination of fully sparse detectors (FSD and FSDv2) as range experts, trained using an adaptive range weighing scheme, and augmenting virtual points to LiDAR data obtained from MVP, a powerful method for image based depth completion. Nevertheless, a large margin for improvement remains for ranges beyond 50 meters. As a future work, our analysis could be extended to other depth completion methods, as well as cover various 3D object detectors. Another possible next step could be investigating whether deep image features could aid sparse LiDAR features for detection, while being computationally efficient. An interesting line of investigation can be studying camera based methods to detect objects beyond the range of current LiDAR sensors.

ACKNOWLEDGMENT

The computations were enabled by the supercomputing resource Berzelius provided by National Supercomputer Centre at Linköping University and the Knut and Alice Wallenberg Foundation, Sweden.

REFERENCES

- [1] S. Shalev-Shwartz, S. Shammah, and A. Shashua, "On a formal model of safe and scalable self-driving cars," *arXiv preprint arXiv:1708.06374*, 2017.
- [2] B. Wilson, W. Qi, T. Agarwal, J. Lambert, J. Singh, S. Khandelwal, B. Pan, R. Kumar, A. Hartnett, J. K. Pontes *et al.*, "Argoverse 2: Next generation datasets for self-driving perception and forecasting," *arXiv preprint arXiv:2301.00493*, 2023.
- [3] Y. Li, L. Fan, Y. Liu, Z. Huang, Y. Chen, N. Wang, Z. Zhang, and T. Tan, "Fully sparse fusion for 3d object detection," *arXiv preprint arXiv:2304.12310*, 2023.
- [4] H. Zhang, D. Yang, E. Yurtsever, K. A. Redmill, and Ü. Özgüner, "Faraway-frustum: Dealing with lidar sparsity for 3d object detection using fusion," in *2021 IEEE International Intelligent Transportation Systems Conference (ITSC)*. IEEE, 2021, pp. 2646–2652.
- [5] S. Gupta, J. Kanjani, M. Li, F. Ferroni, J. Hays, D. Ramanan, and S. Kong, "Far3det: Towards far-field 3d detection," in *Proceedings of the IEEE/CVF Winter Conference on Applications of Computer Vision*, 2023, pp. 692–701.
- [6] L. T. Triess, M. Dreissig, C. B. Rist, and J. M. Zöllner, "A survey on deep domain adaptation for lidar perception," in *2021 IEEE intelligent vehicles symposium workshops (IV workshops)*. IEEE, 2021, pp. 350–357.
- [7] H. Caesar, V. Bankiti, A. H. Lang, S. Vora, V. E. Liong, Q. Xu, A. Krishnan, Y. Pan, G. Baldan, and O. Beijbom, "nusenes: A multimodal dataset for autonomous driving," in *Proceedings of the IEEE/CVF conference on computer vision and pattern recognition*, 2020, pp. 11 621–11 631.
- [8] P. Sun, H. Kretschmar, X. Dotiwala, A. Chouard, V. Patnaik, P. Tsui, J. Guo, Y. Zhou, Y. Chai, B. Caine *et al.*, "Scalability in perception for autonomous driving: Waymo open dataset," in *Proceedings of the IEEE/CVF conference on computer vision and pattern recognition*, 2020, pp. 2446–2454.
- [9] T. Matuszka, I. Barton, Á. Butykai, P. Hajas, D. Kiss, D. Kovács, S. Kunsági-Máté, P. Lengyel, G. Németh, L. Pető *et al.*, "aimotive dataset: A multimodal dataset for robust autonomous driving with long-range perception," *arXiv preprint arXiv:2211.09445*, 2022.
- [10] M. Alibeigi, W. Ljungbergh, A. Tonderski, G. Hess, A. Lilja, C. Lindstrom, D. Motorniuk, J. Fu, J. Widahl, and C. Petersson, "Zenseact open dataset: A large-scale and diverse multimodal dataset for autonomous driving," *arXiv preprint arXiv:2305.02008*, 2023.
- [11] Y. Yan, Y. Mao, and B. Li, "Second: Sparsely embedded convolutional detection," *Sensors*, vol. 18, no. 10, p. 3337, 2018.
- [12] B. Graham and L. Van der Maaten, "Submanifold sparse convolutional networks," *arXiv preprint arXiv:1706.01307*, 2017.
- [13] Y. Chen, J. Liu, X. Zhang, X. Qi, and J. Jia, "Voxelnext: Fully sparse voxelnet for 3d object detection and tracking," in *Proceedings of the IEEE/CVF Conference on Computer Vision and Pattern Recognition*, 2023, pp. 21 674–21 683.
- [14] Y. Zhang, Q. Hu, G. Xu, Y. Ma, J. Wan, and Y. Guo, "Not all points are equal: Learning highly efficient point-based detectors for 3d lidar point clouds," in *Proceedings of the IEEE/CVF Conference on Computer Vision and Pattern Recognition*, 2022, pp. 18 953–18 962.
- [15] X. Jiang, S. Li, Y. Liu, S. Wang, F. Jia, T. Wang, L. Han, and X. Zhang, "Far3d: Expanding the horizon for surround-view 3d object detection," *arXiv preprint arXiv:2308.09616*, 2023.
- [16] L. Fan, F. Wang, N. Wang, and Z.-X. ZHANG, "Fully sparse 3d object detection," *Advances in Neural Information Processing Systems*, vol. 35, pp. 351–363, 2022.
- [17] L. He, X. Ren, Q. Gao, X. Zhao, B. Yao, and Y. Chao, "The connected-component labeling problem: A review of state-of-the-art algorithms," *Pattern Recognition*, vol. 70, pp. 25–43, 2017.
- [18] L. Fan, F. Wang, N. Wang, and Z. Zhang, "FSD V2: Improving Fully Sparse 3D Object Detection with Virtual Voxels," *arXiv preprint arXiv:2308.03755*, 2023.
- [19] C. R. Qi, X. Chen, O. Litany, and L. J. Guibas, "Imvotenet: Boosting 3d object detection in point clouds with image votes," in *Proceedings of the IEEE/CVF conference on computer vision and pattern recognition*, 2020, pp. 4404–4413.
- [20] S. Vora, A. H. Lang, B. Helou, and O. Beijbom, "Pointpainting: Sequential fusion for 3d object detection," in *Proceedings of the IEEE/CVF conference on computer vision and pattern recognition*, 2020, pp. 4604–4612.
- [21] S. Xu, D. Zhou, J. Fang, J. Yin, Z. Bin, and L. Zhang, "Fusionpainting: Multimodal fusion with adaptive attention for 3d object detection," in *2021 IEEE International Intelligent Transportation Systems Conference (ITSC)*. IEEE, 2021, pp. 3047–3054.
- [22] Y. Zhang and T. Funkhouser, "Deep depth completion of a single rgb-d image," in *Proceedings of the IEEE conference on computer vision and pattern recognition*, 2018, pp. 175–185.
- [23] J. Ku, A. Harakeh, and S. L. Waslander, "In defense of classical image processing: Fast depth completion on the cpu," in *2018 15th Conference on Computer and Robot Vision (CRV)*. IEEE, 2018, pp. 16–22.
- [24] T. Yin, X. Zhou, and P. Krähénbühl, "Multimodal virtual point 3d detection," *Advances in Neural Information Processing Systems*, vol. 34, pp. 16 494–16 507, 2021.
- [25] N. Peri, M. Li, B. Wilson, Y.-X. Wang, J. Hays, and D. Ramanan, "An empirical analysis of range for 3d object detection," *arXiv preprint arXiv:2308.04054*, 2023.
- [26] T.-Y. Lin, P. Goyal, R. Girshick, K. He, and P. Dollár, "Focal loss for dense object detection," in *Proceedings of the IEEE international conference on computer vision*, 2017, pp. 2980–2988.
- [27] R. Girshick, "Fast r-cnn," in *Proceedings of the IEEE international conference on computer vision*, 2015, pp. 1440–1448.
- [28] M. Contributors, "MMDetection3D: OpenMMLab next-generation platform for general 3D object detection," <https://github.com/open-mmlab/mmdetection3d>, 2020.
- [29] B. Zhu, Z. Jiang, X. Zhou, Z. Li, and G. Yu, "Class-balanced grouping and sampling for point cloud 3d object detection," *arXiv preprint arXiv:1908.09492*, 2019.
- [30] K. Chen, J. Pang, J. Wang, Y. Xiong, X. Li, S. Sun, W. Feng, Z. Liu, J. Shi, W. Ouyang *et al.*, "Hybrid task cascade for instance segmentation," in *Proceedings of the IEEE/CVF conference on computer vision and pattern recognition*, 2019, pp. 4974–4983.
- [31] T. Yin, X. Zhou, and P. Krahenbuhl, "Center-based 3d object detection and tracking," in *Proceedings of the IEEE/CVF conference on computer vision and pattern recognition*, 2021, pp. 11 784–11 793.
- [32] K. He, G. Gkioxari, P. Dollár, and R. Girshick, "Mask r-cnn," in *Proceedings of the IEEE international conference on computer vision*, 2017, pp. 2961–2969.